CCI Vegetation

Climate Assessment Report

Manuela Balzarolo, Catherine Morfopoulos, Christiaan Van der Tol

November 2025

Distribution list

Author(s)	:	Manuela Balzarolo, Catherine Morfopoulos, Christiaan Van der Tol
Reviewer(s)	:	Else Swinnen
Approver(s)	:	Marin Tudoroiu
Issuing authority	:	VITO

Change record

Release	Date	Pages	Description of change	Editor(s)/Reviewer(s)
V1.0	06/10/2025	all	Revision	Reviewer: Else Swinnen
V1.1	20/10/2025	all	Final document revision and submission	Editor: Manuela Balzarolo
V1.2	20/11/2025	Multiple pages	Editorial changes	Else Swinnen

Executive summary

The objective of the European Space Agency (ESA) Climate Change Initiative (CCI) for the Vegetation Parameters project (https://climate.esa.int/en/projects/vegetation-parameters/) is to provide a global, multi-decadal and multi-sensor time series (2000-2020) of jointly retrieved LAI and fAPAR with demonstrated added value for the climate scientific community, at 1 km and 300 m spatial resolution. This document describes potential climate applications selected by researchers of the Climate Research Group (CRG) to demonstrate the usability of the data produced in the frame of this project for both Cycle-2 and Cycle-1.

The selected use cases (UC) cover the following areas of research:

- UC#1: Assessing the utility of new Leaf Area Index (LAI) and Fraction of Absorbed Photosynthetically Active Radiation (fAPAR) products for detecting seasonality changes focusing.
- UC#2: Exploring the role of the green Fraction of Absorbed Photosynthetically Active Radiation (fAPARgreen or fAPARCab) in detecting ecosystem phenology.
- UC#3: Extreme events. Differences between fAPARCab (or: fAPARgreen), fAPAR and fAPAR carotenoids (fAPARCar).
- UC#4: Climate drivers of ecosystem photosynthesis: fAPAR versus fAPARCab.

UC#1 and UC#2 are concluded using the CRDP-1 dataset. UC#3 and UC#4 are planned and will be developed using the CDRP-2 dataset. ESA CMUG Phenology Team is testing the use of ESA CCI Leaf Area Index (LAI) in land surface modelling and outcomes of this analysis will be reported in the updated version of the CAR by the end of the project.

The results contained in this report were made available to the ESA CCI Vegetation Science Team to improve the data products during the project development. This report will be updated by the end of the project.

Table of Contents

List of Acronyms

ATBD	Algorithm Theoretical Basis Documents
AVHRR	MetOp-A/C-AVHRR
CAR	Climate Assessmant Report
CCI	Climate Change Initiative
CI	Clumping Index
CMUG	Climate Modelling User Group
CONCERTO	Improved Carbon cycle representation through multiscale models and Earth Observation for Terrestrial Ecosystems
COP	Copernicus
CO2	Carbon dioxide
CRDP	Climate Research Data Package
CRG	Climate Research Group
CRO	Croplands
CSH	Closed Shrublands
C3S	Copernicus Climate Change Service
DBF	Deciduous Broadleaf Forests
DoY	Day of the Year
EEO	Eco-Evolutionary Optimality
EBF	Evergreen Broadleaved Forests
ECV	Essential Climate Variables
ENF	Evergreen Needleleaf Forests
EO	Earth Observation
EoS	End Of Season
ESA	European Space Agency
fApar	Fraction of Absorbed Photosynthetically Active Radiation
fAPARcab	Chlorophyll ab component of Fraction of Absorbed Photosynthetically Active Radiation
fAPARcar	Carotenoids component of Fraction of Absorbed Photosynthetically Active Radiation
fAPARgreen	Green component of Fraction of Absorbed Photosynthetically Active Radiation
GCC	Green Chromatic Coordinate
GCOS	Global Climate Observing System
GPP	Gross Primary Productivity
GPPCCI	Gross Primary Productivity modelled by P-model trained with CCI fAPAR
GPPCop	Gross Primary Productivity modelled by P-model trained with Copernicus fAPAR
GPPinsitu	Gross Primary Productivity derived by in situ flux measurements
GRA	Grasslands
ICOS	Integrated Carbon Observation System
IGBP	International Geosphere–Biosphere Programme
LAI	Leaf Area Index
MCD12Q1	MODIS Land Cover Type Product
MF	Mixed Forests
MODIS	Moderate-Resolution Imaging Spectroradiometer
MOS	Maximum of Season
OSH	Open Shrublands
OptiSAIL	Optimized Soil-Canopy Interaction Model

Pa	Atmospheric pressure
PAR	Photosynthetically Active Radiation
PTF	Plant Functional Type
PV	PROBA-V
RMSE	Root Mean Squared Error
RUE	Radiation Use Efficiency
SIF	Solar Induced Chlorophyll Fluorescence
S3	Sentinel-3A and B OLCI
SoS	Start of Season
SW	Shortwave Radiation
TOA	Top-Of-Atmosphere
UC	Use Cases
VGT	SPOT4/5-VEGETATION
VGT1	SPOT4/5-VEGETATION1
VGT2	SPOT4/5-VEGETATION2
VIIRS	S-NPP VIIRS
VPD	Vapor Pressure Deficit
WET	Wetlands
WMO	World Meteorological Organization

List of Figures

List of Tables

1 Introduction

1.1 Scope of the document

This document is the first version of the Climate Assessment Report (CAR) to evaluate the datasets produced in the ESA CCI Vegetation Parameters project, focusing on the first dataset CRDP-1. It summarizes the current activities within the ESA CCI Vegetation Parameters project in the context of CRDP assessment and evaluates the overall usability of the generated products in climate applications. A preliminary description of the activities relevant for climate science is reported and is made thanks to the interactions between the Climate Research Group (CRG) of the ESA CCI Vegetation Parameters project with the Climate Modelling User Group (CMUG) and climate scientific community and stakeholders.

The next update will be in 2026, assessing CRDP v3.0 and CRDP v4.0.

1.2 Structure of the document

This document is organized in the following three sections:

- ESA CCI Vegetation Parameters fAPAR/LAI products (Chapter 2)
- Description of the use cases (Chapter3)
- Conclusions and remarks (Chapter 4)

Chapter 2 gives a summary of the ESA CCI LAI and fAPAR products and the processing chain to generate them. Chapter 3 describes the UC and reports on the outcomes of the applications. Chapter 4 summarizes the main outcomes of the CAR and UC applications.

1.3 Related documents

Table 1 Internal documents.

Reference ID	Document
ID1	Climate Change Initiative Extension (CCI+) Phase 2 New ECVs: Vegetation Parameters – EXPRO+ - Statement of Work, prepared by ESA Climate Office, Reference ESA-EOP-SC-CA-2021-7, Issue 1.2, date of issue 26/05/2021
VP-CCI_D1.1_URD_V2.0	User Requirement Document: fAPAR and LAI, ESA CCI+ Vegetation Parameters https://climate.esa.int/media/documents/VP-CCI_D1.1_URD_V2.0.pdf
VP-CCI_D2.1_ATBD_V2.2	Algorithm Theoretical Basis Document: fAPAR and LAI, ESA CCI+ Vegetation Parameters http://climate.esa.int/media/documents/VP-CCI_D2.1_ATBD_V2.2.pdf
VP-CCI_D4.2_PUG_V2.1	Product User Guide: LAI and fAPAR, ESA CCI+ Vegetation Parameters http://climate.esa.int/media/documents/VP-CCI_D4.2_PUG_V2.1.pdf
VP-CCI_D3.1_SSD_V2.1	System Specifications Document: LAI and fAPAR CCI+ Vegetation Parameters https://climate.esa.int/media/documents/VP-CCI_D3.1_SSD_V2.1.pdf
VP-CCI-SIF_D2.1_ATBD_V1.0	Algorithm Theoretical Basis Document: fAPAR and LAI, ESA CCI+ Vegetation Parameters SIF Processing

Table 2 External documents.

Reference ID	Document
CCI Data Standards	ESA Climate Office, CCI Data Standards v2.3 (CCI-PRGM-EOPS-TN-13-0009
C3S ATBD SA	C3S ATBD of Surface Albedo, multi-sensor, D1.3.4-v2.0_ATBD_CDR_SA_MULTI_SENSOR_v2.0_PRODUCTS_v1.1

1.4 General definitions

Leaf Area Index (LAI) is defined as the total one-sided area of all leaves in the canopy within a defined region, and is a non-dimensional quantity, although units of [m^2/m^2] are often quoted, as a reminder of its meaning (Zemp et al., 2022). The selected algorithm in the CCI-Vegetation Parameters project uses a 1-Dimentional radiative transfer model, and LAI is uncorrected for potential effects of crown clumping. Its value can be considered as an effective LAI, notably the LAI-parameter of a turbid-medium model of the canopy that would let the model have similar optical properties as the true 3-Dimentional structured canopy with true LAI (Pinty et al., 2006). Additional information about the geometrical structure may be required for this correction to obtain true LAI (Nilson, 1971), which involves the estimation of the clumping index (CI) defined as the ratio between the true and effective LAI [see Fang (2021) for a review of methods to estimate CI].

Fraction of Absorbed Photosynthetically Active Radiation (fAPAR) is defined as the fraction of Photosynthetically Active Radiation (PAR; solar radiation reaching the surface in the 400-700 nm spectral region) that is absorbed by a vegetation canopy (Zemp et al., 2022).

2 ESA fAPAR and LAI CCI Vegetation parameters products

2.1 Main product characteristics

This section summarizes the overall workflow applied to generate fAPAR/LAI ESA CCI products. A detailed description of the workflow is provided in the above Table 1 with the description of the related documents.

The processing starts from top-of-atmosphere (TOA) reflectance data (L1B) from SPOT4/5-VEGETATION1/2 (VGT1/2), PROBA-V (PV), Sentinel-3A and B OLCI (S3), MetOp-A/C-AVHRR (AVHRR) and S-NPP VIIRS (VIIRS). All datasets are pre-processed to surface reflectance with the same atmospheric correction and atmospheric input data, thereby propagating and adding uncertainty measures to the surface reflectance. These surface reflectance data with associated uncertainties are then used jointly in the inversion scheme OptiSAIL (Blessing, Giering, et al., 2024) to retrieve LAI and fAPAR simultaneously with information on the uncertainty and covariance between the parameters.

The production and release of CCI VP fAPAR/LAI datasets align with cyclic structure of the ESA CCI Vegetation Parameters project:

- **Cycle 1**: comparison of different retrieval algorithms using data from SPOT VGT and PV for a spatially limited dataset → Realised dataset: Climate Research Data Package 1 (CRDP-1) described in Table 1.
- **Cycle 2**: multi-sensor retrieval by adding all sensors mentioned above and analysing the optimal sensor combination. Algorithm improvements based on the evaluation and user feedback of the first dataset were also implemented. → Realised dataset: Climate Research Data Package 2 (CRDP-2).
- **Cycle 3**, which has not started at the time of the preparation of this report (CAR): focus on the improvement of the processing performance to generate the full global dataset.

Use cases presented in this report focused on the use of the data generated in Cycle 1 and anticipate two new use cases that will be performed to test the use of the CRDP-2 dataset produced in Cycle 2.

Table 3 Description of the Climate Research Data Packages of the CCI Vegetation Parameters project.

Name	***Cycle***	***Resolution***	***Sensors***	***ROI***	***Period***
CRDP-1	*1*	*1000 m*	*SPOT4/5-VGT1/2, PROBA-V*	*Selected sites + transect*	*2000-2020*
CRDP-2	*2*	*1000 m*	*SPOT4/5-VGT1/2, PROBA-V, Sentinel-3 A & B OLCI, Metop-A/C-AVHRR, SNPP-VIIRS*	*Selected sites + transect*	*2000-2020*
CRDP-3	*3*	*1000 m*	*SPOT4/5-VGT1/2, PROBA-V, Sentinel-3 A & B OLCI, Metop-A/C-AVHRR, SNPP-VIIRS*	*Global*	*2000-2020*
CRDP-4	*3*	*300 m*	*Selected sensors from: Terra/Aqua-MODIS, Envisat-MERIS, PROBA-V, Sentinel-3 A & B OLCI*	*Global*	*2000-2020*

2.2 Product availability

The CRDP-1 dataset is already available, and the CRDP-2 dataset will be available around autumn 2025. Data can be accessed and downloaded from the Open Data Portal of ESA (https://climate.esa.int/en/data/#/dashboard).

The DOI of the CRDP-1 data set is http://10.5285/34e4bfe402c048c783e64eac0f0bca37.

The DOI of the CRDP-2 data set is http://10.5285/8d02d224437247f6a6270a575d457bd8 .

More information and the detailed documents can be found on the ESA CCI website https://climate.esa.int/en/projects/vegetation-parameters/.

Two notebooks were prepared to facilitate and demonstrate the use of the data. The notebooks are available on the GitHub through https://github.com/Christiaanvandertol/VegetationCCI.

3 Description of the use cases

3.1 Climate applications and the carbon cycle

Climate and the carbon cycle strongly interact. One of the major challenges in climate scenarios is understanding the response of land sink to climate anomalies (e.g., droughts and heatwaves) and its interannual variability to accurately predict the future behavior of the carbon-climate feedback. To improve this situation, changes in biophysical vegetation properties (e.g. LAI and fAPAR) due to local climate events must be detected in the time series. For this reason, the Global Climate Observation System (GCOS) has set a requirement for daily temporal resolution as a goal in the GCOS- 245 requirements report (WMO, 2022) for LAI and fAPAR as well. This requirement can only be met if observations from multiple satellite platforms are combined in a systematic and consistent manner. To ensure that abrupt changes in time series are preserved, it is also necessary to avoid temporal smoothing of the time series.

The LAI and fAPAR are recognized as Essential Climate Variables (ECV) and their monitoring based on remote sensing observations is a crucial step towards improving climate science. LAI and fAPAR are state variables of multiple interdependent processes, including the light scattering in the foliage, the light absorption, rainfall interception, evaporation, and ecosystem respiration. They are also good indicators of phenology and growth stages (Verger et al., 2016). Besides these two ECV, there is a need for additional observational constraints on photosynthesis, for example solar induced chlorophyll fluorescence (SIF), will enable a closer inspection into the solar energy dissipation pathways following light absorption (Porcar-Castell et al., 2014).

The fAPAR is widely used to estimate GPP (Anav et al., 2015) in global productivity models. However, these products are limited by sensor dependency and insufficient spatio-temporal resolution, making it difficult to capture subtle seasonal changes. At the same time, focusing on the temporal dynamics of GPP seasonality can provide important insights into the variability of carbon sequestration and the mechanisms by which ecosystems absorb CO_2 (Piao et al., 2009). The start (SoS) and end (EoS) of the growing season, combined with vegetation physiological factors, can explain over 90% of the interannual variability in global GPP (Xia et al., 2015). Additionally, an increase in the length of the growing season directly extends the period of net carbon uptake, leading to an increase in annual GPP. Studies have shown that between 1980 and 2002, each additional day in the growing season length in the Northern Hemisphere (> 25°N) resulted in a 0.6% increase in annual GPP (Piao et al., 2019). Therefore, accurate detection of SoS and EoS is extremely important for the carbon balance of terrestrial ecosystems as well as for changes in atmospheric CO_2 concentrations.

With a suite of dynamic global vegetation models, Sitch et al., (2015) found a significant trend towards a higher sink for the period 1990-2009, which was mostly caused by an increase in the leaf area per unit surface area (LAI), thus a higher fraction of absorption of photosynthetically active radiation (fAPAR). The global trend in LAI further appears to be a strong driver of the steady increase in evaporation on land since 1980, even stronger than the influences of increased precipitation due to increased ocean evaporation (Yang et al., 2023). Much less certain is the evolution of the efficiency by which photons are used in the gross primary productivity (the light use efficiency), and responses and trends in ecosystem respiration. Respiration, carboxylation and gas exchange via stomata are usually modelled with (a priori defined) plant functional type parameterization, but there is a need for quantitative empirical evidence of ecosystems adaptation to climate change that can help reduce the dependence on prior parameterization (Brady, 2016).

The new ESA CCI fAPAR and LAI dataset covers 2000-2020 at a 1 km resolution with a 5-day revisit cycle and is retrieved using multiple sensors (SPOT4/5-VEGETATION1/2 and PROBA-V) in the Optimized Soil-Canopy Interaction Model (OptiSAIL). It provides better coherence, temporal resolution, and independent of specific sensors (addressing the issues of short and inconsistent time series). The evaluation of the accuracy through comparisons with reference data (Brown et al., 2020) is crucial. The validation of the product focusses on the comparison with in situ data at specific times or under average conditions (Abuelgasim, Fernandes and Leblanc, 2006). Thus, the new ESA CCI LAI and fAPAR offer a more comprehensive assessment of vegetation data products under varying conditions and seasons, necessary for the synergistic use of remote sensing data and for revealing the underlying mechanisms of matter and energy exchange between terrestrial vegetation systems and the climate (Ge et al., 2015).

3.2 UC#1: Assessing the utility of new Leaf Area Index (LAI) and Fraction of Absorbed Photosynthetically Active Radiation (fAPAR) products for detecting seasonality changes

The aims of UC#1 include:

- Establishing the relationship between P-model-simulated GPP and tower-based GPP, as well as between CCI-simulated GPP and CCI-fAPAR to evaluate the performance of half-hourly GPP estimates during the period of 2000-2019.
- Identifying the most accurate SoS and EoS detection technique for GPP derived from CCI data in alignment with flux tower observations.
- Based on the optimal detection technique, we further analyze SoS and EoS biases at the plant functional types (PFTs) and site levels.

3.2.1 Methods

3.2.1.1 Sites selection

Fifty-five sites were selected from the Integrated Carbon Observation System (ICOS) measurement sites across Europe (https://www.icos-cp.eu/data-services) and FLUXNET2015 database. These flux networks utilize advanced eddy covariance technology and high-precision sensors to provide continuous flux data, employing unified observation protocols and standardized methods across various ecosystems, with open data sharing. The sites were selected on criteria of homogeneity (Figure 1), meaning that they have consistent vegetation cover within flux towers' measurement range and satellite image resolution. The sites span latitudes from 40°N to 70°N and longitudes from 10°W to 40°E, covering various PFTs based on the International Geosphere-Biosphere Programme (IGBP) classification. PFTs were confirmed using the ICOS Data Portal and MODIS Land Cover Type Product (MCD12Q1). Eddy covariance measurements based on ICOS sites were collected and unified in the FLUXNET2015 synthetic database, and the FLUXNET2015 data-processing pipeline methodology consistent with the processing and review of ICOS eddy covariance flux data (https://fluxnet.org/data/fluxnet2015-dataset/) (Pastorello et al., 2020). GPP estimates used were half-hourly GPP night-based (GPP, µmol CO2 m^{-2} s^{-1}). In addition, air temperature (°C), vapor pressure deficit (VPD, hPa), atmospheric pressure (PA, kPa), and shortwave radiation (SW, W/m²) were extracted from the dataset as meteorological input data for the P-model.

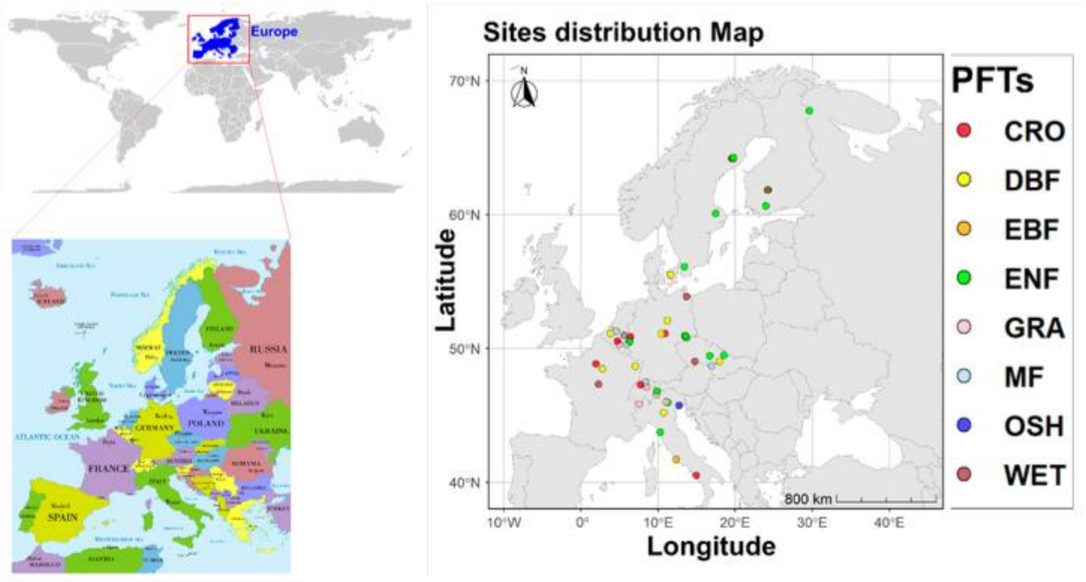

Figure 1: Locations of selected 55 sites across Europe in nine IGBP plant functional types, including: mixed forest (MF, 4 sites), grassland (GRA, 8 sites), deciduous broadleaf forest (DBF, 9 sites), croplands (CRO, 9 sites), closed shrubland (CSH, 1 site), evergreen needleleaf forest (ENF, 17 sites), wetland (WET, 5 sites), evergreen broadleaf forest (EBF, 1 site), open shrubland (OSH, 1 site).

3.2.2 fAPAR products

3.2.2.1 CCI fAPAR

The fAPAR dataset from the European Space Agency, covering 2000-2020 at a 1 km resolution with a 5-day revisit cycle (https://catalogue.ceda.ac.uk/uuid/34e4bfe402c048c783e64eac0f0bca37), is derived from SPOT4/5-VEGETATION1/2 and PROBA-V sensors. fAPAR were retrieved using the Optimized Soil-Canopy Interaction Model (OptiSAIL), encompassing a north-south transect from Finland to South Africa and representative sites of all biomes globally (Clerici et al., 2010; Blessing, Giering and van der Tol, 2024). The fAPAR tested here is from the first cycle — Climate Research Data Packages (CRDP-1). Data underwent linear interpolation, smoothing with a 20-day moving window, and interpolation to generate half-hourly fAPAR as input for sub-daily P-model (GPPCCI). This product is henceforth referred to as simply CCI.

3.2.2.2 Copernicus fAPAR

The global fAPAR 1 km version 2 data were provided by Copernicus Global Land Service (https://land.copernicus.eu/en/products/vegetation/fraction-of-absorbed-photosynthetically-active-radiation-v2-0-1km). Instantaneous fAPAR values are estimated at 10-day intervals from 1999 to 2020 using neural networks trained on CYCLOPES and MODIS products, based on SPOT/VGT (1999 - 2013) and PROBA-V (2014 - 2020) data. This product will henceforth refered to as simply COP.

3.2.2.3 The P-model

The P-model combines the Farquhar–von Caemmerer–Berry model with eco-evolutionary optimality (EEO) principles to represent plant and vegetation processes. The P-model requires the following inputs to estimate GPP: air temperature (°C), vapor pressure deficit (VPD), atmospheric pressure (Pa), and shortwave radiation (W/m²), CO2 concentration (ppm) and fAPAR. Given that ICOS/FLUXNET do not provide annual CO2 data, a mean atmospheric CO2 concentration of 400 ppm was assumed for the inputs. More information about the P-model can be found in (Wang et al., 2017; Stocker et al., 2020). The P-model is implemented in the “pyrealm 0.10.1” Python package, (https://github.com/ImperialCollegeLondon/pyrealm).

3.2.3 Detection of phenology parameters

3.2.3.1 Data preprocessing

To reconstruct gap-filled seasonal trajectories from the annual GPP time series and reduce outliers and noise in SoS and EoS detection, the three GPP datasets (GPPinsitu, GPPCCI and GPPCop) were uniformly pre-processed. Missing values were filled using linear interpolation, followed by a 20-day moving window to smooth the GPP time series.

3.2.3.2 Detection techniques

This study tested common methods for detecting vegetation seasonality parameters (SoS and EoS) from GPP time series:

a. Percentile Thresholds Method: SoS and EoS were defined as the days (day of the year, DoY) when GPP value rose to and fell to given thresholds. The given dynamic thresholds were set based on the annual percentage amplitude of the GPP curve (Verger et al., 2016). We tested 20th, 30th and 50th percentiles of annual amplitudes for SoS, and 30th, 40th and 60th percentiles for EoS.
b. First Derivative Method: SoS and EoS were defined as the DoY of the maximum increase (maximum first derivative) and maximum decrease in the annual GPP curve (Tateishi and Ebata, 2004).
c. Logistic Function: SoS and EoS were identified as the DoY of the first local maximum and minimum rate of change in the curvature of a logistic function fitted to the annual GPP time series (Zhang et al., 2003).

Figure 2 illustrates the workflow of data processing and phenological metrics detection.

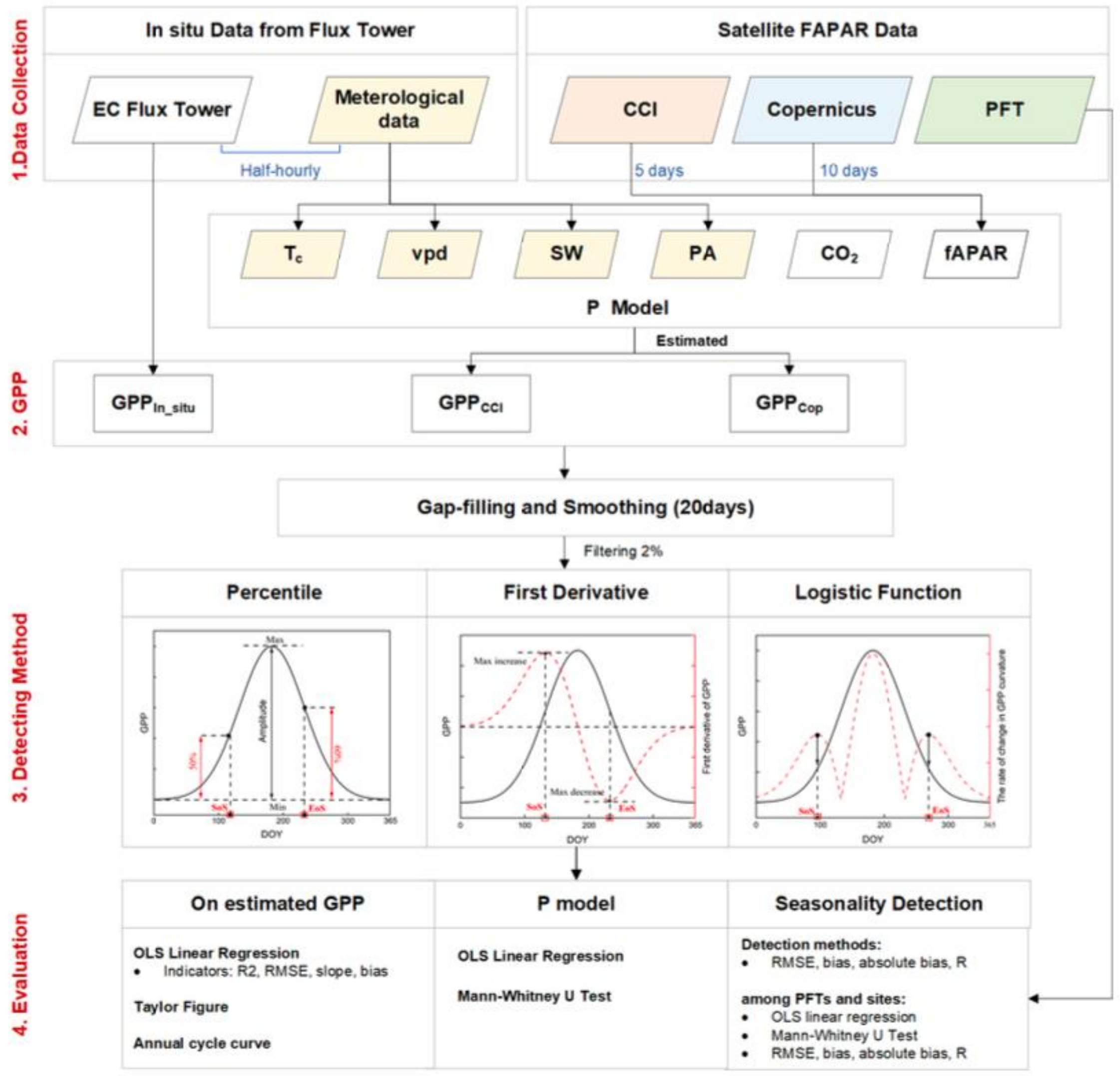

Figure 2: The overall framework of the whole project, the impact of using new fAPAR product of CCI as inputs on the phenological metrics is assessed. The evaluation process includes: 1) data collection; 2) estimating GPP using the P-model; 3) detecting SoS and EoS through 3 methods; 4) evaluating the products and model with statistical metrics and tests.

3.2.4 Results

3.2.4.1 Consistency of GPP simulations

The consistency between the fAPAR and P-model-based GPP is shown in Figure 3 that compares the correlation and seasonality detection bias between CCI fAPAR product and estimated GPPCCI by P-model. There was a significant positive correlation between fAPAR and GPPCCI (p-value < 0.001). In the P-model, 50% ($R^2 = 0.50$) of the variation in GPPCCI was explained by changes in fAPARCCI (Figure 3a). This confirmed that fAPAR was a key driver of GPP variation within the P-model. Across different PFTs, the bias in SoS and EoS timing showed clear systematic differences. Overall, SoS detected by fAPAR tended to occur earlier than in situ by approximately 20 - 60 days, while EoS showed a significant delay of around 20 - 70 days (Figure 3b).

3.2.4.2 Consistency between simulated GPP with in situ GPP

Figure 3 illustrates that whether forced by CCI (Figure 3a) or COP (Figure 3b) fAPAR, the predicted daily GPP values from the P-model showed a significant linear relationship with observed GPP across 55 ICOS flux tower sites. This indicated that the GPP time series estimated using fAPAR and the P-model can accurately reproduce the GPP observations from the flux towers. Even though the Copernicus data performed slightly better (R^2 = 0.67, RMSE = 2.64) than the CCI data (R^2 = 0.60, RMSE = 2.84), the difference is not substantial. The Taylor diagram shows that both the CCI and Copernicus data had a significant positive correlation with in-situ GPP measurements, with 12 correlation coefficients close to 0.8. From the average intra-annual seasonal variation trends across all study sites (Figure 3c), it was evident that the three datasets exhibited a high degree of consistency, with an upward trend from spring to summer and a downward trend from summer to autumn, featuring a single peak between days 150 and 200. Although GPPCCI values were closer to GPPinsitu compared to GPPCop, the overall trend showed greater divergence, particularly given the lag observed in both P-model estimates. The figure showed that the peak timing in the CCI data lagged significantly behind the in situ measurements, whereas the Copernicus data peak aligned much more closely with the in situ data. Additionally, given the noticeable noise in the three GPP seasonal curves, it was necessary to smooth the GPP data before detecting SoS and EoS.

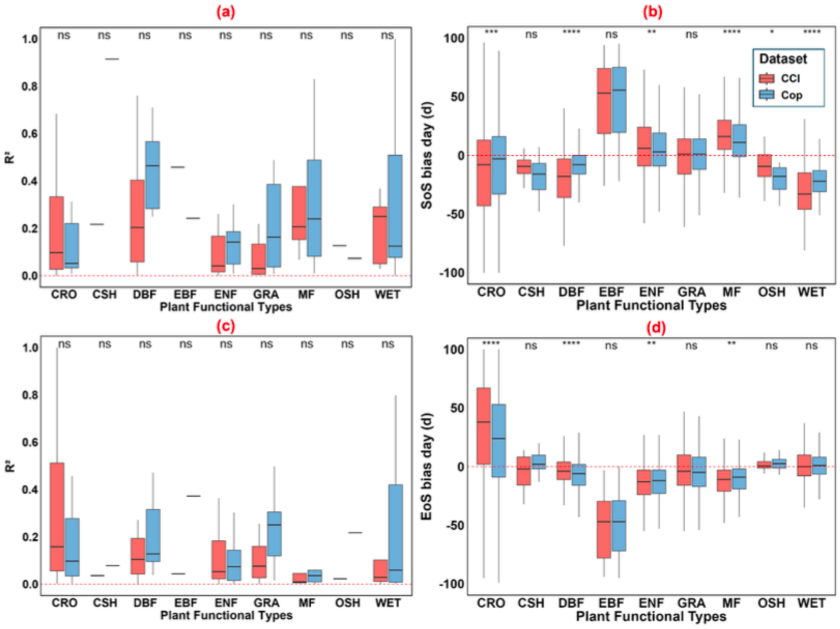

*Figure 3: Comparison of R^2 values and bias days for Start of Season (SoS) and End of Season (EoS) across nine vegetation types using GPPCCI (red) and GPPCop (blue) datasets against ground-based observations, including data from 2000-2019 and all sites. Panels (a) and (c) illustrate the R^2 values for SoS and EoS, respectively, while panels (b) and (d) depict the corresponding bias days. The short lines indicate vegetation types where only one site was available for analysis. Asterisks (*) mark significant differences between CCI and COP da-taset. 'ns' means no significant difference. Significance levels: * $p < 0.05$, ** $p < 0.01$, *** $p < 0.001$, **** $p < 0.0001$.*

3.2.4.3 Sensitivity analysis of the methods to detect phenology metrics

Table 4 illustrates that the SoS and EoS extracted using each of the methods for the two different fAPAR datasets were significantly positively correlated with the field observations overall. The GPP data threshold-based extraction methods showed superior performance over the first derivative and logistic function fitting methods on the CCI data and Copernicus data, with lower bias and RMSE values.

In the threshold-based methods, the best agreement with ground measurements for the timing of SoS was found for the 50% threshold of GPPCCI amplitude and 30% of GPPCop, with RMSEs of 23.53 and 23.07 days, respectively. For EoS, the estimates defined by the 60% annual amplitude threshold showed the highest accuracy in matching in situ data (RMSE up to 26 days). However, even the best-performing SoS detection method still resulted in an RMSE as high as 23 days, and the best EoS estimate had an even higher RMSE (26 days) and absolute error (20 days) compared to SoS. Under the same percentile method, GPPCop generally outperformed GPPCCI in terms of RMSE and bias for both SoS and EoS. Compared to in situ measurements, the average SoS detected by the optimal percentile method was delayed by 6 days (GPPCCI) and 7 days (GPPCop), while the average EoS was delayed by 8 days (GPPCCI) and 6 days (GPPCop). These results indicated that, although GPPCop slightly outperformed in detecting SoS and EoS, both remote sensing datasets showed relatively close performance in terms of bias, with both exhibiting a certain degree of temporal lag. Therefore, given that this study primarily evaluated the CCI data, the detection methods that best matched the ground observations — percentile 50% for SoS and percentile 60% for EoS — were selected for further evaluation of CCI data in detecting phenological metrics across different PFTs and sites in the next section.

3.2.4.4 Sensitivity analysis among PFTs

Figure 3a and c illustrate the distribution of R^2 values for SoS and EoS across different PFTs. Most paired site R^2 values fell between 0 and 0.6, but there were significant differences in performance across vegetation types. In DBF, ENF, and WET, the R^2 values for SoS ranged widely, indicating considerable differences in prediction accuracy between sites. In contrast, the R^2 values for EoS were more consistent across most PFTs and ranged between 0.1 and 0.6. *Table 4* contains the complete linear regression parameters for each PFT.

The bias analysis of SoS and EoS across different PFTs revealed notable differences simulated GPP(s) compared to in situ data. For SoS, biases in ENF and GRA were relatively small (± 20 days) but could reach up to 70 days in CRO and EBF. EoS biases were generally within ± 20 days in CSH, GRA, OSH, and WET, closely aligning with in situ measurements, but can reach up to 50 days in CRO and EBF. The asterisks (*) indicated CCI generally showed greater bias than COP.

Notably, in GRA, SoS bias relative to in situ measurements was nearly zero, but the extended 'whiskers' indicated that even within the same PFT, there was significant site-level variation in bias days. This variation was also evident in the analysis of EoS (GRA and WET). Given this bias, the following section will address site-level bias analysis.

3.2.4.5 Sensitivity analysis among sites

Overall, there were significant differences in the sensitivity to SoS and EoS detection across flux tower sites (Figure 4). At most sites, the absolute bias between P-model estimates and flux tower data for SoS and EoS was less than 30 days, with only a few sites showing a bias of 5 days or less. For EoS, however, COP data tended to show an earlier signal for both EoS and SoS at more sites, while CCI data exhibited more severe delays (bias > 30 days) (Figure 4). This suggests that COP data generally aligned better with ground-based phenological indicators, although CCI data could still perform well at some sites where COP estimates were less accurate.

To further identify seasonal variations and error sources in different datasets at individual sites, Figure 4e-f show mean annual GPP curves and phenological points for six typical sites, highlighting cases of severe advancement (bias < 30 days), general consistency (|bias| < 5 days), and severe delay (bias > 30 days). GPPCCI and GPPCop generally followed similar mean annual distribution to GPPin_situ, with a single peak during the growing season, reflecting high summer productivity in Europe consistent with typical Northern Hemisphere vegetation patterns. The degree of bias depends on the consistency of change rates across GPP time-series curves, and the temporal bias of SoS and EoS was determined by trends in the ascending and descending portions of the curves, not directly by the absolute GPP error (e.g., FR-Fon, IT-SR2). Notably, the accuracy of SoS and EoS based on satellite GPP time-series detection was more affected when the field data curves exhibited a double-peak structure (IT-BCi), showed significant fluctuations (IT-BFt and CH-Oe2), or when the peaks were not clearly defined (IT-Cp2). The double-peak structure often observed in croplands, may have been due to two growth peaks, such as early growth after sowing and the grain-filling stage (when the grain begins to swell and accumulate nutrients). Satellite products may have struggled to accurately capture these complex growth patterns, leading to errors. However, SoS and EoS biases may vary at the same site. For instance, at CH-Oe2, EoS from satellite data was significantly delayed (bias > 30 days), while SoS bias was less than 5 days.

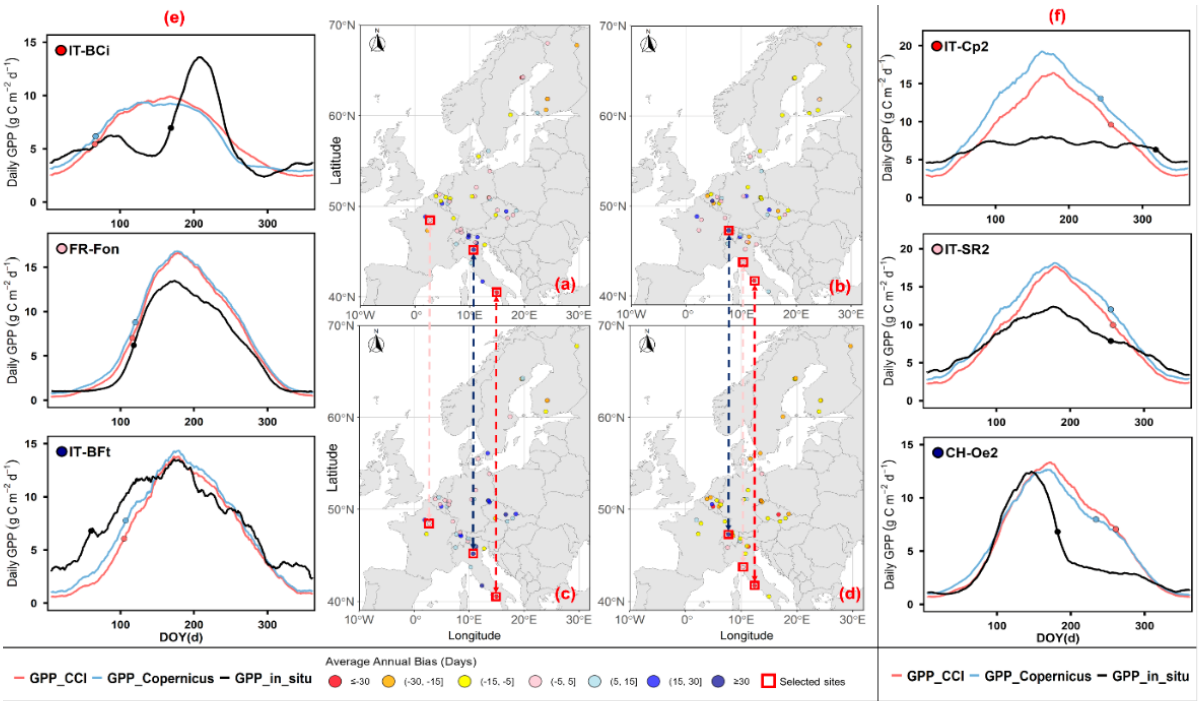

Figure 4: The comparison of SoS and EoS bias across 55 ICOS sites, along with average annual GPP curves at selected sites, is presented as follows: Panels (a) and (b) depict the difference in average SoS and EoS days between the CCI and in-situ observations, with bias levels indicated by color. Similarly, panels (c) and (d) show the SoS and EoS bias using COP data. In panels (e) and (f), the daily average GPP curves at six representative sites

3.2.5 Conclusions

Although the P-model-simulated GPP and tower-based GPP exhibit a significant linear correlation, notable SoS and EoS biases exist, especially in CRO and EBF. These biases may stem from random errors in flux tower measurements and systematic errors in satellite products. Since the fAPAR data relies on sensor inputs, several common bias sources may impact the consistency of seasonal detection in both datasets.

Mismatch in spatial scales is a common issue when validating remote sensing phenology using ground-based observations. Low spatial resolution can result in detected greening dates appearing earlier for the understory compared to the forest canopy by up to 21 days (Augspurger, Cheeseman and Salk, 2005). Despite CCI and COP data having a 1 km resolution, this scale still does not align well with the flux towers' observational range, which only spans tens to hundreds of meters (Rebmann et al., 2018). Although the project assumes homogeneity of PFTs within the remote sensing pixel sampling area, the 1 km resolution actually captures a composite response from multiple vegetation types and phenological behaviors. This means that fAPAR values might be influenced by vegetation outside the flux tower's observation range, leading to different values than those within the actual footprint, thereby causing early-season lag bias in the simulations (as shown in Figure 4, simulated GPP > tower-based)

(Maleki et al., 2020). However, this situation is not absolute and can vary depending on the vegetation diversity within the pixel.

Beyond spatial mismatches, phenology detection is highly sensitive to the chosen method. Among the three advanced methods tested, the first derivative and logistic function approaches showed lower agreement with ground-measured phenophases, consistent with previous studies (Bórnez et al., 2020).

The first derivative method is particularly sensitive to noise in time series, performing poorly in shorter growing seasons and often misidentifying phenophases during rapid and abrupt changes or double peaks (Beck et al., 2006). The logistic function method, although widely used (Zhang et al., 2003), depends heavily on model fitting quality and may fail when curvature is too flat to determine SoS and EoS (Beck et al., 2006; de Beurs and Henebry, 2010). In contrast, the amplitude percentile threshold method is more robust but still sensitive to noise-affected amplitudes (Max-Min values). Overall, each method has specific limitations, with no single method proving superior in all cases. Therefore, future research should expand the analysis to a broader range of vegetation types, adjust algorithms to accommodate different growth cycles, and develop real-time phenology prediction systems.

Phenological indicator detection is highly sensitive to the quality of satellite datasets. Previous studies have shown that uncertainties in satellite data quality, such as solar angles during autumn and winter, atmospheric effects, and cloud contamination, typically result in lower alignment of EoS with ground data compared to SoS (Delbart et al., 2005). Additionally, soil background effects and vegetation canopy structure (e.g., leaf angle, distribution, orientation, and density) can influence the spectral response of remote sensing data (Maleki et al., 2020). Systematic errors such as sensor calibration, solar elevation angle, and algorithm differences may also contribute to inconsistencies with in-situ data and among different satellite datasets.

This study found that the EoS dates detected directly from fAPAR data were significantly delayed compared to in-situ GPP observations, while SoS dates were noticeably advanced Figure 4b. The EoS delay may occur because the P-model's GPP is driven by fAPAR, reflecting canopy greenness. However, a time lag between detected greenness and actual photosynthesis, especially at the start and end of the growing season, can lead to bias. (Maleki et al., 2020; Stocker et al., 2020). Therefore, the EoS delay is likely caused by the fAPAR product itself. Notably, the P-model has significantly improved the early SoS and delayed EoS issues observed in fAPAR products (Figure 3).

However, in certain vegetation types (CRO and EBF), there may be overcorrection, which corresponds with the low correlation observed in GPP estimates discussed in section 3.1. In this study, COP data generally outperformed the CCI dataset in describing phenophases, showing lower bias and higher R^2 in detecting SoS and EoS. While low temporal resolution can affect phenology estimation (Zhang et al., 2017), COP's 10-day data performed better than CCI's 5-day data. This suggests that systematic errors in satellite datasets or noise in the time series may impact accuracy more than temporal resolution. Also, higher temporal resolution is more susceptible to climate variability, noise, and random errors.

This study confirms that P-model-simulated GPP, derived from both CCI and Copernicus data, is significantly correlated with tower-based GPP at ICOS sites. However, the goodness of fit varied significantly across different PFTs. The optimal GPP amplitude thresholds for detecting SoS and EoS were 30th and 40th for SoS, and 50th for EoS. It is important to note that these results are geographically limited, and adjustments to the thresholds may be necessary for applications in other regions or for specific PFTs or species. Additionally, both satellite datasets showed substantial bias in detecting seasonality compared to in-situ measurements, likely due to spatial resolution mismatches, variations in satellite product quality, and random errors in tower observations. The P-model generally improved the early SoS and delayed EoS observed in most vegetation types, though reverse biases occurred in some PFTs. This evaluation underscores the potential of new fAPAR products and the P-model in phenology detection, offering valuable insights for addressing current limitations and enhancing the integration of remote sensing data in climate science and carbon cycle research, ultimately supporting a deeper understanding of earth's biogeochemical cycles.

*Table 4: Statistics of comparisons between GPPCCI and GPPCop from P-model derived phenology for SoS and EoS, and the ground flux tower measurements for three methods (percentiles, first derivative and logistic function). *Mark indicates the results are at the significant correlations level at $p < 0.05$ (** indicates $p < 0.001$). First and Logistic means first derivative and logistic function respectively.*

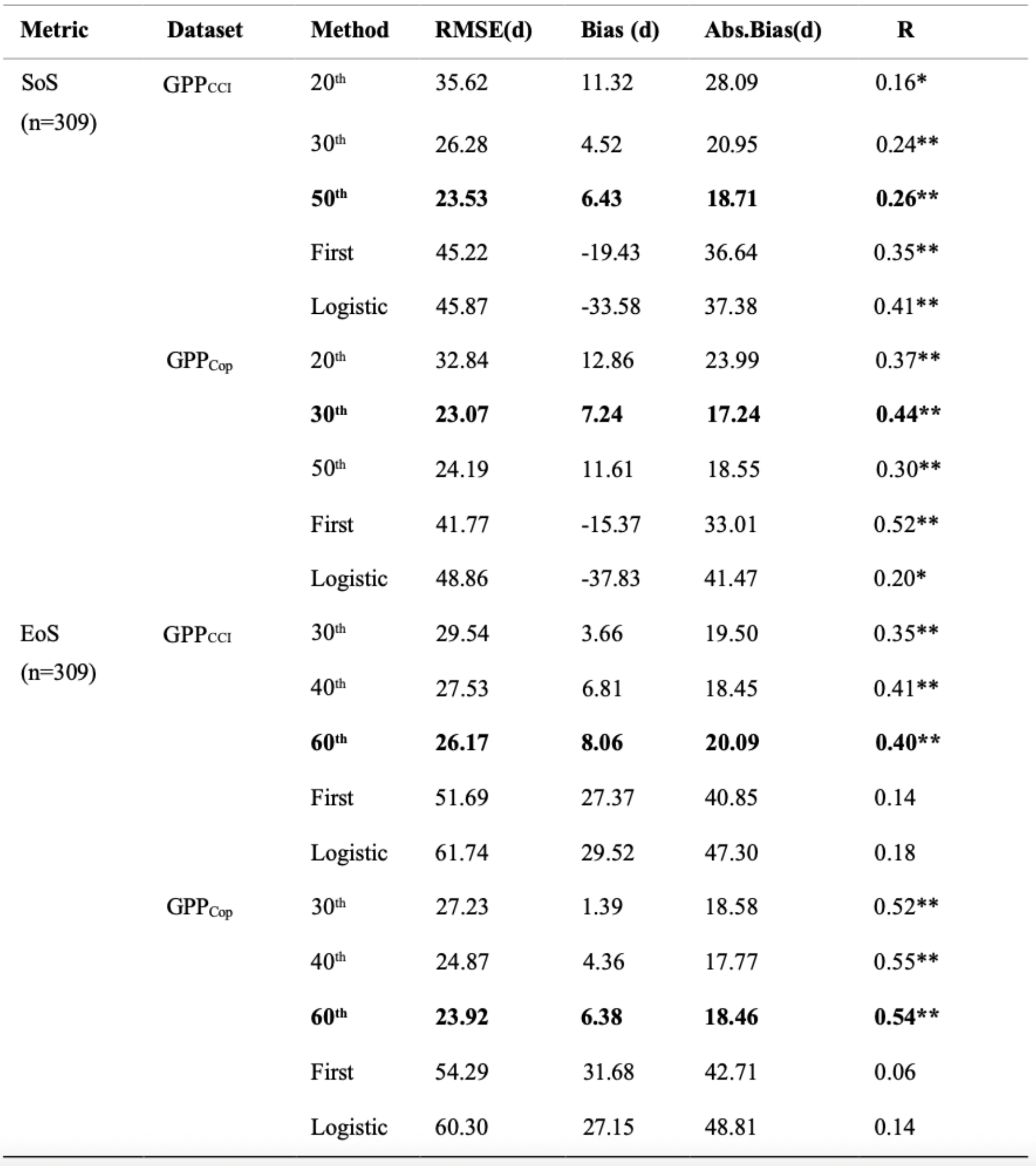

Metric	Dataset	Method	RMSE(d)	Bias (d)	Abs.Bias(d)	R
SoS (n=309)	GPP$_{CCI}$	20th	35.62	11.32	28.09	0.16*
		30th	26.28	4.52	20.95	0.24**
		50th	**23.53**	**6.43**	**18.71**	**0.26****
		First	45.22	-19.43	36.64	0.35**
		Logistic	45.87	-33.58	37.38	0.41**
	GPP$_{Cop}$	20th	32.84	12.86	23.99	0.37**
		30th	**23.07**	**7.24**	**17.24**	**0.44****
		50th	24.19	11.61	18.55	0.30**
		First	41.77	-15.37	33.01	0.52**
		Logistic	48.86	-37.83	41.47	0.20*
EoS (n=309)	GPP$_{CCI}$	30th	29.54	3.66	19.50	0.35**
		40th	27.53	6.81	18.45	0.41**
		60th	**26.17**	**8.06**	**20.09**	**0.40****
		First	51.69	27.37	40.85	0.14
		Logistic	61.74	29.52	47.30	0.18
	GPP$_{Cop}$	30th	27.23	1.39	18.58	0.52**
		40th	24.87	4.36	17.77	0.55**
		60th	**23.92**	**6.38**	**18.46**	**0.54****
		First	54.29	31.68	42.71	0.06
		Logistic	60.30	27.15	48.81	0.14

3.3 UC#2: The role of the green Fraction of Absorbed Photosynthetically Active Radiation (fAPAR) in detecting ecosystem phenology

Canopy phenology has been widely studied using a range of methodologies across various spatial and temporal scales. The earliest methods involved field observations of individual species which were complemented later by measurements of leaf area index (LAI) and fAPAR within small experimental plots. Recently, near-surface remote sensing techniques—such as flux measurements and digital repeat photography—have enabled automated observations and expanded the monitoring of canopy development and phenology (Hufkens et al. 2012). Satellite-based proxy of canopy greenness (e.g.

fAPAR) and LAI images show the most recent advances in ecosystem phenology studies, extending the spatial scale to continents and the temporal scale to decades. All these approaches differ methodologically and are thus subject to varying degrees of heterogeneity in species composition, space, and time.

The ESA CCI dataset also provides the additional vegetation products of green fAPAR which is the portion of APAR absorbed by chlorophyll, and leaf chlorophyll albedo in the spectral regions.
In the UC#2 we investigated the use of phenological metrics derived from fAPAR to describe the carbon-flux phenology, acknowledging that the timing of fAPAR derived phenology is not necessarily equal to that of GPP-derived phenology. The fAPAR greenness phenology and carbon phenology in the time series were quantified by the timing of the start, maximum and end of the seasonal GPP cycle (SoS, MOS and EoS, respectively).

Phenocam images offer observational phenology data that integrate satellite data in the description of the vegetation response to stresses (e.g. altered timing of greening, earlier leaf senescence, suppressed growth) improving the description of the ecosystem carbon flux anomalies during climate- and anthropogenic-induced stresses. From phenocam images, the canopy phenological metrics (e.g. green-up, senescence) are derived from green chromatic coordinate (GCC) index (Hufkens et al., 2018). In this use case we used phenocam images as a benchmark method to test the ability of fAPARgreen to capture the canopy changes. The phenocam images for the ICOS sites used were downloaded from the ICOS Carbon Portal. Sites and years with large gaps were excluded from further analysis. Daily records of the 90th percentile of the GCC data from phenocams were collected for the ICOS sites selected for this study. The 90th percentile was used to minimize atmospheric effects on the daily GCC record.

3.3.1 Detection of flux (GPP) and greenness (canopy) phenology parameters

3.3.1.1 Data preprocessing

The starting day of greening (Start-of-Season, SoS) was estimated using:

- fAPAR and fAPARCab from this ESA CCI
- in situ webcam observations
- In situ flux GPP from selected sites used in the UC#1

The phenological metrics for each timeseries and flux site was derived applying the Savitzky–Golay smoothing method a threshold method using TIMESAT software (Jönsson & Eklundh, 2004; http://www.nateko.lu.se/TIMESAT/timesat.asp) and as described in Balzarolo et al. (2016). In detail, we used the adaptive Savitzky-Golay method for time-series smoothing and the double sigmoid method to extract seasonally dependent variables from a time series. A double sigmoid was fitted through each smoothed time-series of data. The phenological parameters (e.g., SoS and SOE and the amplitude of the curve) were extracted by the threshold method as implemented in TIMESAT. The SoS was defined, using the double sigmoid function to determine the time (day) corresponding with 20% of the time-series amplitude, defined as the distance between the time series left side minimum and maximum levels. The EoS was defined similarly starting in that case from the time-series right side minimum.

Among the datasets available from the ESA Climate Change Initiative (CCI) Vegetation Parameters, the fAPAR and fAPAR_Cab products effectively capture the start of season (SoS) of canopy greenness in temperate deciduous forests, as derived from in situ webcam observations (Figure 5). Both proxies indicate an earlier SoS and a later end of season (EoS) compared to gross primary production (GPP). This discrepancy arises because greenness-based proxies do not directly respond to the primary environmental drivers of photosynthesis, such as soil moisture (Maleki et al., 2020) and temperature, which were not included in the present analysis. Nevertheless, all proxies accurately characterize the peak of the growing season (MOS). The reliability of phenological metrics derived from these proxies is influenced by the choice of smoothing functions and extraction methods, which can introduce temporal lags in detecting the onset of leaf green-up and senescence relative to underlying eco-physiological changes (Mariën et al., 2019). Therefore, alternative processing approaches should be considered to assess the sensitivity of phenological estimates, enabling more accurate quantification of both carbon flux and canopy greenness phenology (Maleki et al., 2020; Panwar et al., 2023).

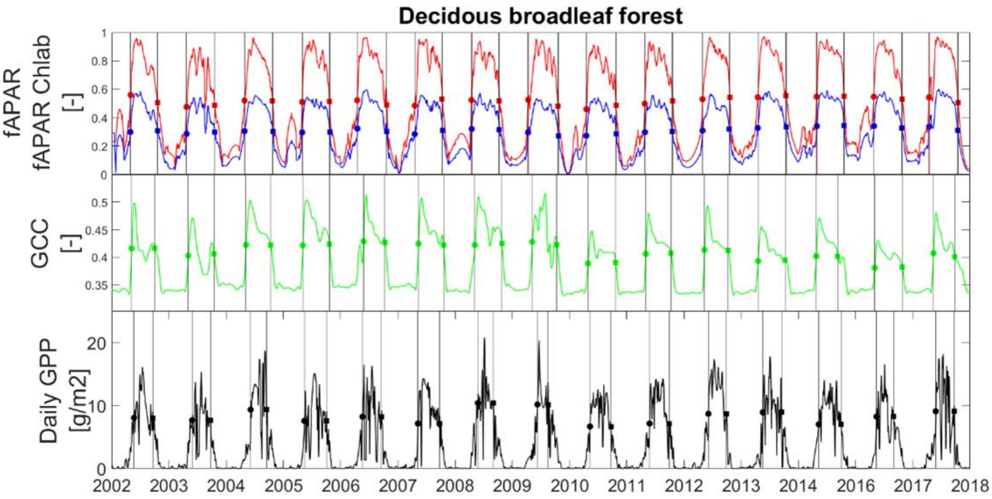

Figure 5: Example of timeseries of (upper panel) fAPARCab, (middle) greenness derived from webcam observations (GCC – Green Chromatic Coordinate), and (c) Gross Primary Productivity (GPP) for a deciduous forest in Germany. Phenological metrics extracted from each timeseries are represented by filled dots and squares for the start of the season (SoS) and the end of the season (EoS).

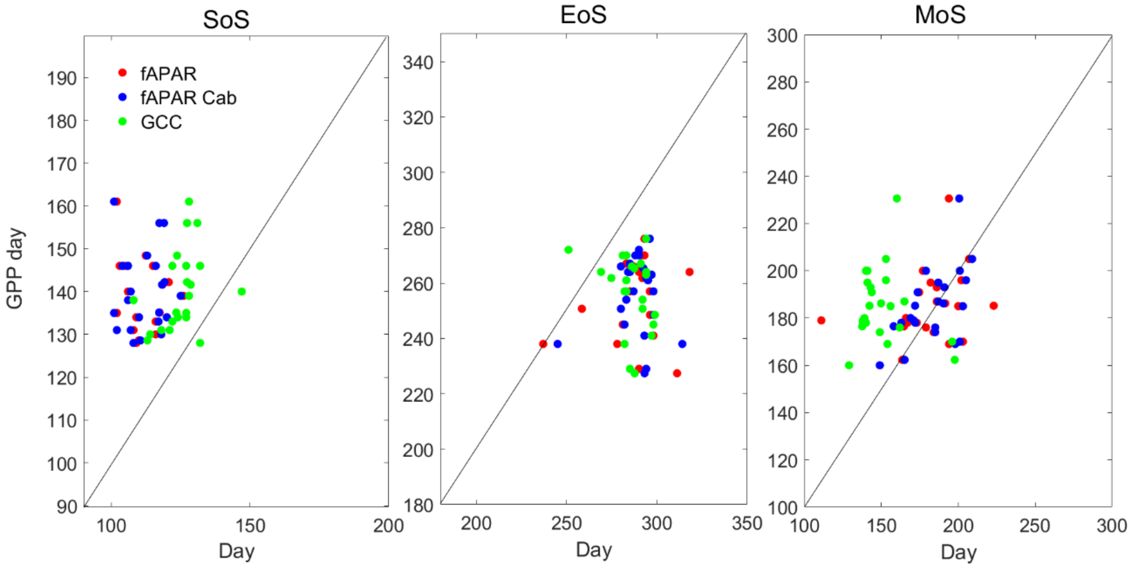

Figure 6: Scatterplot between SoS, EoS and MoS extracted from GPP and derived from fAPAR, fAPAR-Cab and GCC for temperate forests in Europe.

3.4 UC#3: Extreme events. Differences between fAPARCab (or: fAPARgreen), fAPAR and fAPAR carotenoids (fAPARCar)

Extremes play a critical role in the carbon cycle, as they can either enhance or weaken the terrestrial carbon sink. With heatwaves and droughts being projected to increase in frequency under future climate scenarios, the occurrence of such extremes is expected to rise. It is therefore essential to have reliable satellite products capable of monitoring these events. In this study, we propose to evaluate the ability of the new fAPAR product to track extreme events across space. We will investigate extreme in the fAPARgreen (or fAPARCab) and total fAPAR products, examining whether differences arise between vegetation extremes detected by fAPARgreen versus those detected by standard fAPAR. Specifically, we aim to assess whether these products capture different types of extreme events, the extent to which they track climatic extremes, and whether they may also reflect changes in land cover (e.g., deforestation). To address these questions, we will analyse transect data over the whole period and apply methods proposed by Zscheischler et al. (2013) to track extremes using satellite data. These methods have also been used to track extreme events in the formaldehyde column by Morfopoulos et al. (2022) (Figure 7).

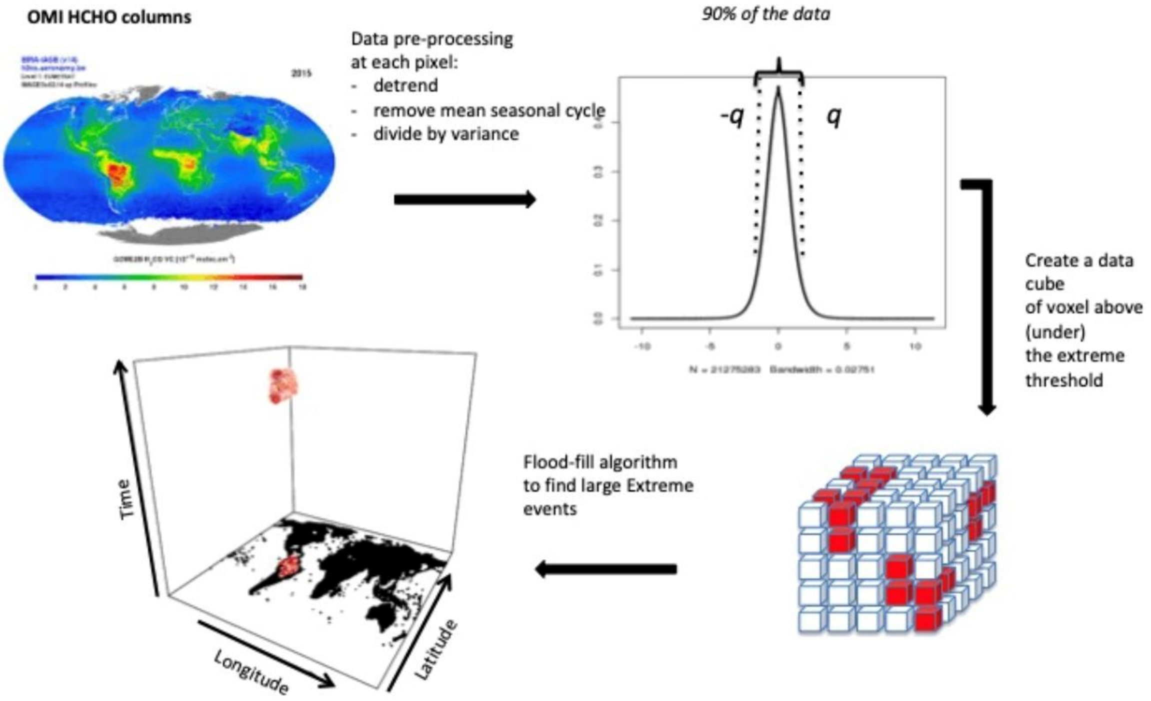

Figure 7: Method of detection of extremes in OMI-HCHO columns (shown here for the first extreme corresponding to the 2015 El Niño event over South America).

3.5 UC#4: Climate drivers of carbon cycle: fAPAR versus fAPARCab

The global ecological modeling and the remote sensing communities are particularly interested in the radiation use (RUE) concept which represents the efficiency of the vegetation to transform absorbed light energy into organic compounds (GPP/APAR = GPP/(APAR*fAPAR). However, it is not fully understood if (and how) models should simulate RUE in function of environmental factors. To do this, first it is needed to find suitable proxies that capture well RUE variability in space (from local to global) and in time (from daily to annual). RUE changes over time because GPP is affected by the current environmental conditions and because the absorbed radiation is affected by changes in incident PAR and leaf properties (e.g. leaf and chloroplast movement) which can occur over short-time scale. In this use case we propose to investigate the role of the fAPARgreen in the estimation of radiation use efficiency.

4 Conclusions and remarks

This document reports on the UCs developped by the Climate Reseach Group (CRG) of the ESA CCI Vegetation Parameters. It showed the results of the test study using the CDPR-1 database released in the project. New applications will be done on the CDPR-2 dataset in the next cycle of the project and the results of the new applications will be reported in the updated version of the CAR by the end of the project.

The CRG contributed to the writing of a chapter of a book submitted to Elsevier for a book on satellite data products. The book chapter contains a study on phenology, which relates to the UC#2 of the CRG. The CGR participates in CMUG meetings focusing on phenology. The use of the new ESA CCI fAPAR product is promoted by CRG in the frame of the EU CONCERTO project, coordinated by Manuela Balzarolo, expert of the CRG.

5 References

Abuelgasim, A.A., Fernandes, R.A. and Leblanc, S.G. (2006) 'Evaluation of national and global LAI products derived from optical remote sensing instruments over Canada', IEEE Transactions on Geoscience and Remote Sensing, 44(7), pp. 1872–1884. Available at: https://doi.org/10.1109/TGRS.2006.874794.

Anav, A. et al. (2015) 'Spatiotemporal patterns of terrestrial gross primary production: A review', Reviews of Geophysics, 53(3), pp. 785–818. Available at: https://doi.org/10.1002/2015RG000483.

Augspurger, C.K., Cheeseman, J.M. and Salk, C.F. (2005) 'Light Gains and Physiological Capacity of Understorey Woody Plants during Phenological Avoidance of Canopy Shade', Functional Ecology, 19(4), pp. 537–546.

Balde, H. et al. (2023) 'Synergy between TROPOMI sun-induced chlorophyll fluorescence and MODIS spectral reflectance for understanding the dynamics of gross primary productivity at Integrated Carbon Observatory System (ICOS) ecosystem flux sites', Biogeosciences, 20(7), pp. 1473–1490. Available at: https://doi.org/10.5194/bg-20-1473-2023.

Beck, P.S.A. et al. (2006) 'Improved monitoring of vegetation dynamics at very high latitudes: A new method using MODIS NDVI', Remote Sensing of Environment, 100(3), pp. 321–334. Available at: https://doi.org/10.1016/j.rse.2005.10.021.

Beer, C. et al. (2010) 'Terrestrial Gross Carbon Dioxide Uptake: Global Distribution and Covariation with Climate', Science, 329(5993), pp. 834–838. Available at: https://doi.org/10.1126/science.1184984.

de Beurs, K.M. and Henebry, G.M. (2010) 'Spatio-Temporal Statistical Methods for Modelling Land Surface Phenology', in I.L. Hudson and M.R. Keatley (eds) Phenological Research: Methods for Environmental and Climate Change Analysis. Dordrecht: Springer Netherlands, pp. 177–208. Available at: https://doi.org/10.1007/978-90-481-3335-2_9.

Blessing, S., Giering, R. and van der Tol, C. (2024) 'OptiSAIL: A system for the simultaneous retrieval of soil, leaf, and canopy parameters and its application to Sentinel-3 Synergy (OLCI+SLSTR) top-of-canopy reflectances', Science of Remote Sensing, 10, p. 100148. Available at: https://doi.org/10.1016/j.srs.2024.100148.

Bloomfield, K.J. et al. (2023) 'Towards a General Monitoring System for Terrestrial Primary Production: A Test Spanning the European Drought of 2018', Remote Sensing, 15(6), p. 1693. Available at: https://doi.org/10.3390/rs15061693.

Booth, B.B.B. et al. (2012) ‘High sensitivity of future global warming to land carbon cycle processes’, Environmental Research Letters, 7(2), p. 024002. Available at: https://doi.org/10.1088/1748-9326/7/2/024002.

Bórnez, K. et al. (2020) ‘Land surface phenology from VEGETATION and PROBA-V data. Assessment over deciduous forests’, International Journal of Applied Earth Observation and Geoinformation, 84, p.101974. Available at: https://doi.org/10.1016/j.jag.2019.101974.

Brown, L.A. et al. (2020) ‘Evaluation of global leaf area index and fraction of absorbed photosynthetically active radiation products over North America using Copernicus Ground Based Observations for Validation data’, Remote Sensing of Environment, 247, p. 111935. Available at: https://doi.org/10.1016/j.rse.2020.111935.

Canadell, J.G. et al. (2000) ‘Commentary: Carbon Metabolism of the Terrestrial Biosphere: A Multitechnique Approach for Improved Understanding’, Ecosystems, 3(2), pp. 115–130. Available at: https://doi.org/10.1007/s100210000014.

Clerici, M. et al. (2010) ‘Consolidating the Two-Stream Inversion Package (JRC-TIP) to Retrieve Land Surface Parameters From Albedo Products’, IEEE Journal of Selected Topics in Applied Earth Observations and Remote Sensing, 3(3), pp. 286–295. Available at: https://doi.org/10.1109/JSTARS.2010.2046626.

Cox, P. and Jones, C. (2008) ‘Illuminating the Modern Dance of Climate and CO2’, Science, 321(5896), pp. 1642–1644. Available at: https://doi.org/10.1126/science.1158907.

De Beurs, K.M. and Henebry, G.M. (2005) ‘Land surface phenology and temperature variation in the International Geosphere–Biosphere Program high-latitude transects’, Global Change Biology, 11(5), pp. 779–790. Available at: https://doi.org/10.1111/j.1365-2486.2005.00949.x.

Delbart, N. et al. (2005) ‘Determination of phenological dates in boreal regions using normalized difference water index’, Remote Sensing of Environment, 97(1), pp. 26–38. Available at: https://doi.org/10.1016/j.rse.2005.03.011.

Duveiller, G. and Cescatti, A. (2016) ‘Spatially downscaling sun-induced chlorophyll fluorescence leads to an improved temporal correlation with gross primary productivity’, Remote Sensing of Environment, 182, pp. 72–89. Available at: https://doi.org/10.1016/j.rse.2016.04.027.

Ge, Q. et al. (2015) ‘Phenological response to climate change in China: a meta-analysis’, Global Change Biology, 21(1), pp. 265–274. Available at: https://doi.org/10.1111/gcb.12648.

Griebel, A. et al. (2020) ‘Generating Spatially Robust Carbon Budgets From Flux Tower Observations’, Geophysical Research Letters, 47(3), p. e2019GL085942. Available at: https://doi.org/10.1029/2019GL085942.

Grossiord, C. et al. (2017) ‘Warming combined with more extreme precipitation regimes modifies the water sources used by trees’, New Phytologist, 213(2), pp. 584–596. Available at: https://doi.org/10.1111/nph.14192.

Guanter, L. et al. (2014) ‘Global and time-resolved monitoring of crop photosynthesis with chlorophyll fluorescence’, Proceedings of the National Academy of Sciences, 111(14), pp. E1327–E1333. Available at: https://doi.org/10.1073/pnas.1320008111.

Guimberteau, M. et al. (2018) ‘ORCHIDEE-MICT (v8.4.1), a land surface model for the high latitudes: model description and validation’, Geoscientific Model Development, 11(1), pp. 121–163. Available at: https://doi.org/10.5194/gmd-11-121-2018.

Janssens, I.A. et al. (2003) ‘Europe’s Terrestrial Biosphere Absorbs 7 to 12% of European Anthropogenic CO2 Emissions’, Science, 300(5625), pp. 1538–1542. Available at: https://doi.org/10.1126/science.1083592.

Kross, A. et al. (2011) ‘The effect of the temporal resolution of NDVI data on season onset dates and trends across Canadian broadleaf forests’, Remote Sensing of Environment, 115(6), pp. 1564–1575. Available at: https://doi.org/10.1016/j.rse.2011.02.015.

Lasslop, G. et al. (2012) ‘On the choice of the driving temperature for eddy-covariance carbon dioxide flux partitioning’, Biogeosciences, 9(12), pp. 5243–5259. Available at: https://doi.org/10.5194/bg-9-5243-2012.

Lu, X. et al. (2018) ‘Comparison of Phenology Estimated from Reflectance-Based Indices and Solar-Induced Chlorophyll Fluorescence (SIF) Observations in a Temperate Forest Using GPP-Based Phenology as the Standard’, Remote Sensing, 10(6), p. 932. Available at: https://doi.org/10.3390/rs10060932.

Luo, X. et al. (2018) ‘The impact of the 2015/2016 El Niño on global photosynthesis using satellite remote sensing’, Philosophical Transactions of the Royal Society B: Biological Sciences, 373(1760), p. 20170409. Available at: https://doi.org/10.1098/rstb.2017.0409.

Madani, N. et al. (2021) ‘The Impacts of Climate and Wildfire on Ecosystem Gross Primary Productivity in Alaska’, Journal of Geophysical Research: Biogeosciences, 126(6), p. e2020JG006078. Available at: https://doi.org/10.1029/2020JG006078.

Maleki, M. et al. (2020) ‘Estimation of Gross Primary Productivity (GPP) Phenology of a Short-Rotation Plantation Using Remotely Sensed Indices Derived from Sentinel-2 Images’, Remote Sensing, 12(13), p. 2104. Available at: https://doi.org/10.3390/rs12132104.

Meek, D.W. et al. (1984) ‘A Generalized Relationship between Photosynthetically Active Radiation and Solar Radiation’, Agronomy Journal, 76(6), pp. 939–945. Available at: https://doi.org/10.2134/agronj1984.00021962007600060018x.

Mengoli, G. et al. (2022) ‘Ecosystem Photosynthesis in Land-Surface Models: A First-Principles Approach Incorporating Acclimation’, Journal of Advances in Modeling Earth Systems, 14(1), p. e2021MS002767.Available at: https://doi.org/10.1029/2021MS002767.

Nemani, R.R. et al. (2003) ‘Climate-Driven Increases in Global Terrestrial Net Primary Production from 1982 to 1999’, Science, 300(5625), pp. 1560–1563. Available at: https://doi.org/10.1126/science.1082750.

Pastorello, G. et al. (2020) The FLUXNET2015 dataset and the ONEFlux processing pipeline for eddy covariance data’, Scientific Data, 7(1), p. 225. Available at: https://doi.org/10.1038/s41597-020-0534-3.

Piao, S. et al. (2009) ‘Spatiotemporal patterns of terrestrial carbon cycle during the 20th century’, Global Biogeochemical Cycles, 23(4). Available at: https://doi.org/10.1029/2008GB003339.

Piao, S. et al. (2019) ‘Plant phenology and global climate change: Current progresses and challenges’, Global Change Biology, 25(6), pp. 1922–1940. Available at: https://doi.org/10.1111/gcb.14619.

Prentice, I.C. et al. (2014) ‘Balancing the costs of carbon gain and water transport: testing a new theoretical framework for plant functional ecology’, Ecology Letters, 17(1), pp. 82–91. Available at: https://doi.org/10.1111/ele.12211.

Pugh, T.A.M. et al. (2019) ‘Role of forest regrowth in global carbon sink dynamics’, Proceedings of theNational Academy of Sciences, 116(10), pp. 4382–4387. Available at: https://doi.org/10.1073/pnas.1810512116.

Rascher, U. et al. (2015) ‘Sun-induced fluorescence – a new probe of photosynthesis: First maps from the imaging spectrometer HyPlant’, Global Change Biology, 21(12), pp. 4673–4684. Available at: https://doi.org/10.1111/gcb.13017.

Rebmann, C. et al. (2018) ‘ICOS eddy covariance flux-station site setup: a review’, International Agrophysics, 32(4), pp. 471–494. Available at: https://doi.org/10.1515/intag-2017-0044.

Sabbatini, S. et al. (2018) ‘Eddy covariance raw data processing for CO2 and energy fluxes calculation at ICOS ecosystem stations’, International Agrophysics, 32(4), pp. 495–515. Available at: https://doi.org/10.1515/intag-2017-0043.

Stocker, B.D. et al. (2018) ‘Quantifying soil moisture impacts on light use efficiency across biomes’, New Phytologist, 218(4), pp. 1430–1449. Available at: https://doi.org/10.1111/nph.15123.

Stocker, B.D. et al. (2020) ‘P-model v1.0: an optimality-based light use efficiency model for simulating ecosystem gross primary production’, Geoscientific Model Development, 13(3), pp. 1545–1581. Available at:https://doi.org/10.5194/gmd-13-1545-2020.

Tateishi Corresponding author, R. and Ebata, M. (2004) ‘Analysis of phenological change patterns using 1982–2000 Advanced Very High Resolution Radiometer (AVHRR) data’, International Journal of Remote Sensing, 25(12), pp. 2287–2300. Available at: https://doi.org/10.1080/01431160310001618455.

Ulsig, L. et al. (2017) ‘Detecting Inter-Annual Variations in the Phenology of Evergreen Conifers Using Long-Term MODIS Vegetation Index Time Series’, Remote Sensing, 9(1), p. 49. Available at: https://doi.org/10.3390/rs9010049.

Verger, A. et al. (2016) ‘Vegetation baseline phenology from kilometric global LAI satellite products’, Remote Sensing of Environment, 178, pp. 1–14. Available at: https://doi.org/10.1016/j.rse.2016.02.057.

Vicca, S. et al. (2016) ‘Remotely-sensed detection of effects of extreme droughts on gross primary production’, Scientific Reports, 6(1), p. 28269. Available at: https://doi.org/10.1038/srep28269.

Wang, H. et al. (2017) ‘Towards a universal model for carbon dioxide uptake by plants’, Nature Plants, 3(9), pp. 734–741. Available at: https://doi.org/10.1038/s41477-017-0006-8.

Welp, L.R. et al. (2011) ‘Interannual variability in the oxygen isotopes of atmospheric CO2 driven by El Niño’, Nature, 477(7366), pp. 579–582. Available at: https://doi.org/10.1038/nature10421.

White, M.A. et al. (2009) ‘Intercomparison, interpretation, and assessment of spring phenology in North America estimated from remote sensing for 1982–2006’, Global Change Biology, 15(10), pp. 2335–2359. Available at: https://doi.org/10.1111/j.1365-2486.2009.01910.x.

Wohlfahrt, G. et al. (2018) ‘Sun-induced fluorescence and gross primary productivity during a heat wave’, Scientific Reports, 8(1), p. 14169. Available at: https://doi.org/10.1038/s41598-018-32602-z.

Xia, J. et al. (2015) ‘Joint control of terrestrial gross primary productivity by plant phenology and physiology’, Proceedings of the National Academy of Sciences, 112(9), pp. 2788–2793. Available at: https://doi.org/10.1073/pnas.1413090112.

Zhang, X. et al. (2003) ‘Monitoring vegetation phenology using MODIS’, Remote Sensing of Environment, 84(3), pp. 471–475. Available at: https://doi.org/10.1016/S0034-4257(02)00135-9.

Zhang, X. et al. (2017) ‘Exploration of scaling effects on coarse resolution land surface phenology’, Remote Sensing of Environment, 190, pp. 318–330. Available at: https://doi.org/10.1016/j.rse.2017.01.001.

Zhang, Z. et al. (2022) ‘Improved estimation of global gross primary productivity during 1981–2020 using the optimized P model’, Science of The Total Environment, 838, p. 156172. Available at: https://doi.org/10.1016/j.scitotenv.2022.156172.

Zhao, M. and Running, S.W. (2010) ‘Drought-Induced Reduction in Global Terrestrial Net Primary Production from 2000 Through 2009’, Science, 329(5994), pp. 940–943. Available at: https://doi.org/10.1126/science.1192666.